Applied Thermal Engineering 77 (2015) 65–75

Contents lists available at ScienceDirect

Applied Thermal Engineering

journal homepage: www.elsevier.com/locate/apthermeng

Research paper

Performance enhancement of ejector–absorption cooling cycle by re-arrangement of solution streamlines and adding RHE

Azher M. Abed [a, b, *], M.A. Alghoul [a, *], R. Sirawn [a], Ali Najah Al-Shamani [a], K. Sopian [a]

[a] Solar Energy Research Institute (SERI), Universiti Kebangsaan Malaysia, 43600 Bangi, Selangor Malaysia
[b] Department of Air Conditioning and Refrigeration, Al-Mustaqbal University College, Babylon, Iraq

HIGHLIGHTS

- COP enhancement of a flash tank-ejector–absorption cooling cycle by efficient heat recovery.
- Overall COP enhancement is 12.2%, COP increment with the new arrangement of solution streams is 8%.
- COP increment and cooling capacity with added RHE are 4.2% and 4.85%, respectively.
- After modification, the cycle shows a lower generator thermal load and higher evaporator thermal load.
- Applying a statistical paired *t*-test, an extremely significant "cycles performance difference" is confirmed.

ARTICLE INFO

Article history:
Received 4 June 2014
Accepted 1 December 2014
Available online 9 December 2014

Keywords:
Ejector-flash tank-absorption cooling cycle
NH_3/H_2O
Re-arrangement of solution streamlines
Adding RHE
Energy balance analysis
COP enhancement

ABSTRACT

Performance of ejector-flash tank-absorption cooling system working with NH_3/H_2O is still subject for further enhancement. The aim of this study is to optimize the utilization of the internal heat recovery of the system. Two modifications are considered, namely, a new arrangement of solution streamlines between the absorber and generator and adding a refrigerant heat exchanger (RHE) between the condenser and evaporator. Energy balance analysis is performed to compare the COP enhancement of the proposed cycle before and after modification. The COP of the proposed cycle after modification showed a significant COP enhancement about 12.2%. The COP increment with the new arrangement of the solution streamlines and adding RHE are 8% and 4.2% respectively. The results show that the cooling capacity increment of the proposed cycle with added RHE is 4.85%. Moreover, the results showed that the proposed cycle significantly reduced the generator thermal load and increased slightly the evaporator thermal load (i.e., cooling effect) compare to the cycle before modification.

1. Introduction

Refrigeration cycles are the predominant compressors in current applications. However, absorption cycles represent a viable alternative to the compressor cycles because of their relatively lower electricity consumption. This condition is achieved mostly by swapping out the compressor with a thermo-mechanical version. A thermo-mechanical compressor initiates the absorption of refrigeration vapor into the absorption liquid and also increases the solution pressure. Its advantages over other compressors are as follows: its simplest cycle is the single-effect type, low electricity consumption (i.e., 5% of the cooling capacity) because of its ability to use low temperature heat as a driver to produce cold [1,2], the utilization of external thermal energy through renewable resources (i.e., solar radiation and biomass combustion), and the usage of ammonia–water and lithium bromide–water solutions as refrigerants [3,4]. This advantage lowers the usage of hazardous refrigerants in compressors (i.e., greenhouse gases). Despite these purported advantages, its disadvantages include requiring a complex assembly, as well as a larger size and area to function. These reasons explain why absorption cycles are utilized in industrial settings more than anywhere else. The coefficient of performance (COP) for the absorption cooling system is also significantly lower than those for vapor compression systems, which has restricted their wide application. At present, more effort is required to improve their performance and reliability to promote and extend

* Corresponding authors. Solar Energy Research Institute (SERI), Universiti Kebangsaan Malaysia, 43600 Bangi, Selangor Malaysia.
E-mail addresses: azhermuhson@gmail.com (A.M. Abed), dr.alghoul@gmail.com (M.A. Alghoul).

http://dx.doi.org/10.1016/j.applthermaleng.2014.12.003
1359-4311/

Nomenclature

A_t	cross sectional area at nozzle throat (m^2)
A_k	cross sectional area at diffuser-inlet (m^2)
COP	coefficient of performance
h	enthalpy (kJ/kg)
m'	mass flow rate (kg/s)
P	pressure (kPa)
Q	heat capacity (kW)
RCI	relative capacity change index
RHE	refrigerant heat exchanger
SHE	solution heat exchanger
T	temperature (°C)
T_{abs}	absorber temperature (°C)
T_{cond}	condenser temperature (°C)
T_{evp}	evaporator temperature (°C)
T_{gen}	generator temperature (°C)
v	specific volume (kg)
W	pump work (kW)
X	solution concentration
Y	vapor solution concentration
ε	effectiveness of heat exchanger
ω	flow entrainment ratio, secondary stream to primary stream

Subscripts

a	absorber
c	condenser
e	evaporator
g	generator
Ft	flash tank
me	mechanical
v	vapor solution
l	liquid solution
s	solution
r	pure refrigerant NH_3
rect	rectifier
nohx	no heat exchanger
BC	basic cycle
1–17	state points

their use in industrial and commercial applications. These efforts are worthwhile because of the significant benefits that these systems can provide. They can recover waste heat, lower CO_2 emissions by decreasing the electricity demand, mitigate the ozone layer depletion caused by CFC and HCFC refrigerants used in compression refrigeration systems, and spread the use of solar energy by developing solar cooling systems [5]. In enhancing the COP and cooling capacity of an absorption refrigerator, combined absorption/vapor compression cycles have been suggested by many authors [6–8].

The ejector application in a solar refrigeration system has been growing rapidly using different working fluids [12–15]. Previous studies demonstrated that the COP of absorption and ejector refrigerators is in the range of 0.5–0.8, whereas the basic absorption cycle is from 0.2 to 0.6 [1,11].

Combining the ejector with the single stage absorption cycle shows a potential COP improvement of the cycle [9], COPs as high as 0.86–1.04 were observed. The advantage of using an ejector refrigerator cycle is that it can utilize thermal energy at temperature levels higher than 333 K [10]. Heat energy at these temperatures is available from the absorber of the absorption refrigerator. Another advantage of the combined ejector-absorption cycle is that it can work under a triple pressure level, which is able to operate at a lower circulation ratio, lower generator temperature, and higher condenser and absorber temperatures [16,17].

The flash tank is usually added to the multi pressure/stage systems to improve the COP, and increase the cooling capacity. The effect of adding the flash tank in refrigeration and heat pump systems has been previously studied [18–23]. These systems showed an improvement on the cooling and heating effect, which consequently increased the overall COP. The most efficient way to remove flash gas would be to separate it continuously as it forms, and then remove it before completing its expansion. This separation occurs when the upward velocity of the vapor is low enough for the liquid particles to drop back into the tank [24]. In a single-effect cooling system, Sirwan et al. [25,26] investigated the addition of a removable flash tank between the condenser and evaporator in the combined ejector absorption cycle and how it can improve the entrainment ratio of the ejector, along with improving the cooling effect inside the evaporator.

Another device that provides the same results as flash–gas removal is “intercooling”. Intercooling in a refrigeration system can be accomplished with a water-cooled heat exchanger or by using refrigerant. The alternate method uses liquid refrigerant from the condenser to perform the intercooling. The influence of liquid–gas heat exchangers on the system performance and system capacity over a range of operation conditions (i.e., evaporating and condensing) using a number of alternative refrigerants was illustrated and quantified in Refs. [27,28]. The liquid–gas heat exchanger depends on a combination of operating conditions and fluid properties, such as heat capacity, latent heat, and coefficient of thermal expansion [29]. The latent heat of ammonia is only about half that of water, so, for the same duty, the refrigerant and absorbent mass circulation rates are roughly double that of water/lithium bromide. As a result, the sensible heat loss associated with heat exchanger approaches is greater [30]. Accordingly, ammonia/water cycles incorporate more techniques to reclaim sensible heat, described in Hanna et al. [31]. The most increment COP is found approximately 8% by using these RHE's (refrigerant subcooler) [32].

The solution heat exchanger (SHE) is advantageous also, because it cools down the weak solution coming from the generator then heats up the strong solution entering the generator [33]. Kaynakli and Kilic [34] investigated numerically the effect of operating temperature and the effectiveness of the heat exchangers in the basic ARS on the thermal loads of the components, the coefficient of performance (COP, COP_c), and the efficiency ratio (η) with water/lithium bromide. The results showed that the SHE affected the investigated parameters more than the refrigerant heat exchanger (RHE). The SHE increased COP to a maximum of 44%, whereas the RHE increased this value by only 2.8%.

The approach to utilize the heat recovery by rearrangement of the streamlines at the solution heat exchanger and at the rectifier in combined power and cooling cycles was studied in previous researches [37–39]. Cycles with an absorber-heat-recovery mechanism were studied theoretically using various working fluids, namely, NH_3/H_2O and $LiNO_3/NH_3$ by Refs. [35,36]; an approximately 10% improvement in COP was observed using the absorber-heat-recovery mechanism.

Based on the above discussion, this study attempts to apply two modifications in the combined absorption–ejector cooling system.

The first modification allows efficient utilization of the internal heat recovery between the generator and absorber by exchanging the strong solution heat coming from the absorber with the rectifier and increases the strong solution temperature to be generated as well. It also exchanges and recovers the heat of the weak solution through the solution heat exchanger (SHE). This modification optimizes the generator, absorber, and rectifier efficiency. The second modification adds a refrigerant heat exchanger (RHE) between the evaporator and flash tank to enable the cold vapor from the evaporator to exchange its heat with liquid refrigerant coming from the condenser or flash tank to the evaporator and lower its temperature. This modification can optimize the evaporator and flash tank efficiencies.

This study will cover the conceptual and mathematical design of the proposed system, and compares it performance with previous studies. Energy balance analysis is performed to quantify the potential of the proposed cycle.

2. Materials and methods

The binary mixture of NH_3/H_2O and pure NH_3 are used in the proposed system. The detailed thermodynamic property equations of NH_3/H_2O were determined by Bourseau and Bugarel [37], as well as Pátek and Klomfar [40]. These properties (i.e., pressure, temperature, concentration, enthalpy, and density) are necessary for the simulation to calculate the heat and mass balance for the proposed cycle.

A computer program was developed to evaluate the performance of the system using NH_3/H_2O as the working fluid. The mass balances, energy balances, and equations of state for the NH_3/H_2O solution, as well as the refrigerant at each component involved in the cycle are required for system simulation. For the purpose of simulation and analysis, the following assumptions are made:

1 The system operates under a steady-state condition.
2 The concentration of NH_3 leaving the rectifier is 0.996 (state point 2).
3 The refrigerant leaving the condenser and evaporator is saturated (state points 4 and 9).
4 The NH_3/H_2O solution in the generator, rectifier, SHE, and absorber are in the equilibrium state at their respective pressures and temperatures. They are also assumed at a saturated state.
5 The frictional pressure drop in the cycle is neglected except through the expansion device.
6 The flow inside the ejector is steady and 1D. The ejector walls are adiabatic.
7 The primary and secondary flows are saturated, and their velocities are negligible before entering the ejector (states 2 and 17 in Fig. 2, respectively). The velocity of the mixed flow leaving the ejector (at state 3) is also neglected.
8 The ejector geometry parameters and mathematical modeling with the assumption are calculated based on the work of Sun et al. [10] and Sirwan et al. [25].

3. Conceptual design of the proposed cycle

The basic working principle for the combined flash–ejector absorption cooling cycle is described in Fig. 1. The cycle use ammonia–water mixtures as the working fluid, which lowers the heat transfer irreversibility, especially for low temperature finite heat sources such as heat from solar collectors and geothermal heat. The component of the combined absorption–flash tank-ejector cooling system consists of the basic cycle components besides the ejector, rectifier and flash tank.

To optimize the performance of the combined cycle shown in Fig 1, this section will detail the modifications that are suggested in the proposed cycle in Fig. 2.

3.1. Re-arrangement of liquid solution streamlines

Generator temperature should be designed carefully with the properties of the used solution. The generator temperature is designed to heat the strong solution until the minimum ammonia concentration is achieved. Also, a higher weak solution temperature going to the absorber will decrease the absorber efficiency. Moreover, the strong solution received by the generator should be at a saturated temperature to allow the ammonia to evaporate immediately in the generator. Therefore, the strong solution can be partially heated by allowing heat exchange with the rectifier and (SHE).

The new rearrangement of strong solution streamlines is shown in Fig. 2. The ammonia mixture leaves the absorber (state 11) as a saturated solution of low pressure with a relatively high ammonia concentration. It is pumped at high pressure (state 12) and divided

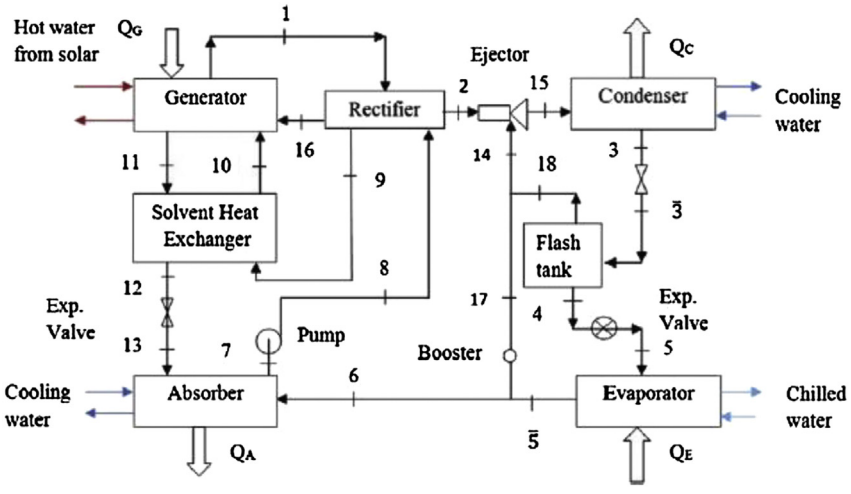

Fig. 1. Combined flash tank–absorption–ejector cooling system [25].

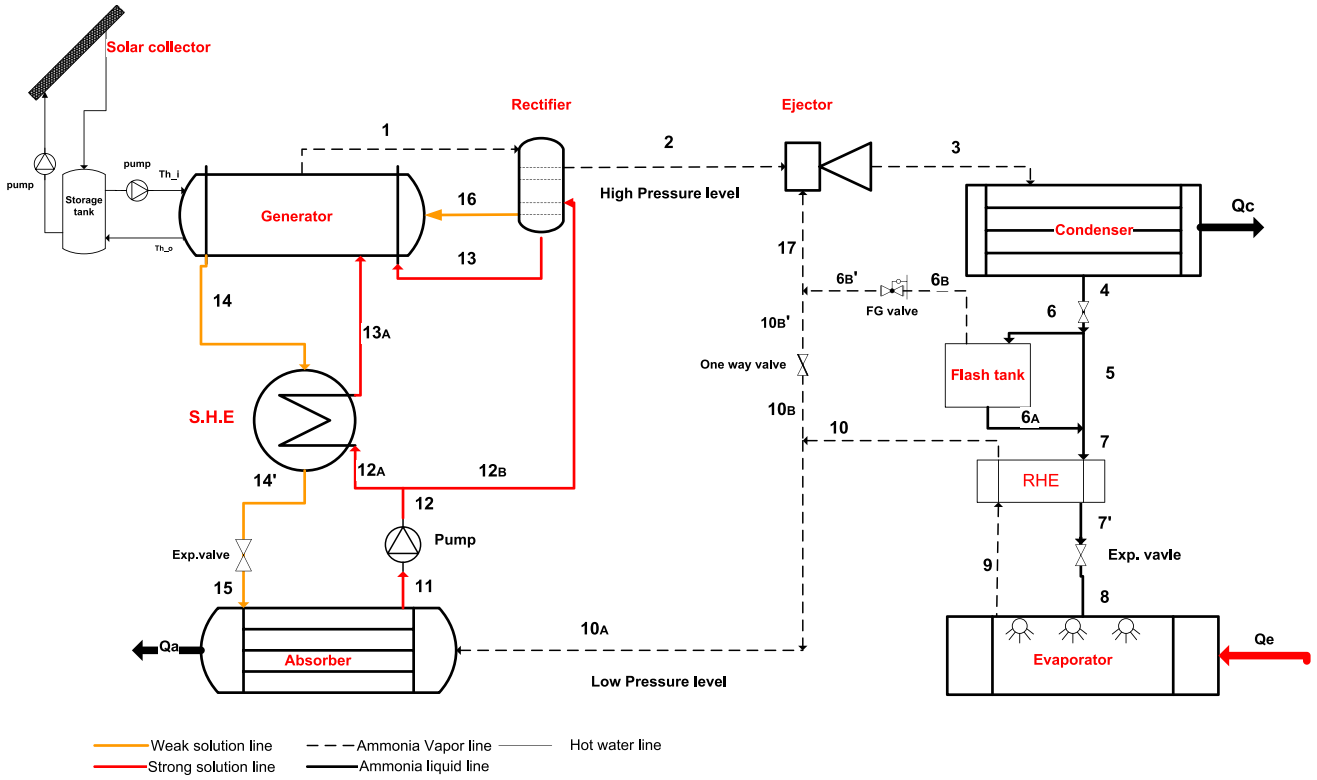

Fig. 2. The schematic diagram of the proposed modified cycle.

into two streamlines. One part flows to the SHE (state 12A) where it is used to exchange the heat with the weak solution (state 14) coming from the generator before entering the absorber, whereas the remaining part flows to the rectifier (state 12B). At the rectifier, the generator vapor (state 1) is cooled by the strong solution pumped from the absorber. This heat exchange will allow small increasing in strong solution temperature (state13). However, usually the rectifier cools the saturated ammonia vapor (state 2) to condense out any remaining water (state 16). The ammonia vapor concentration that left the rectifier and passes to the ejector is 99.6%. This internal rearrangement of heating and cooling of the strong and weak solution would reduce the thermal load of generator and absorber and produce more pure ammonia vapor.

3.2. Refrigerant heat exchanger (RHE)

In the combine ejector – flash tank absorption cycle [25], the COP of the system decreases as the evaporator temperature increases. This limitation is found due to more energetic secondary stream pushes the flow towards the constant section, that results in increasing the exit pressure. When the secondary pressure increases or backpressure decreases, the entrainment ratio will be increased, but any increase over the optimum design will cause reduction in the performance of the ejector [25]. The secondary and primary pressures are the functions of condensing, generating and evaporating temperatures. Usually these temperatures depend on the operating condition and are fixed within a range. Therefore, to overcome this problem, the booster is removed from the combined cycle of [25] and a new arrangement of refrigerant streamlines is performed besides adding FG valve and RHE.

Liquid–gas heat exchangers are commonly installed in refrigeration systems with the intent of ensuring proper system operation and increasing system performance. Specifically, ASHRAE [30] stated that liquid–suction heat exchangers are effective in the following:

1 Increasing the system performance.
2 Subcooling liquid refrigerant to prevent flash gas formation at inlets to expansion devices.
3 Fully evaporating any residual liquid prior to reaching the absorber.

In the combined flash–ejector absorption cooling system as studied in Ref. [25], the flash tank is working as an accumulator and intercooler device of liquid refrigerant coming from condenser. Where this condensed liquid stream undergoes a reduction in pressure by passing through a throttling valve to the flash tank. The flash tank also acts as a vapor separator device to help the evaporator to receive only pure liquid; this vapor will be later sucked by the ejector. Fig. 3 show the schematic diagram of the flash tank.

It is worthy to mention that adjusting FG valve is essential to create an identical pressure with evaporator pressure, and to enable the flash tank working properly. If the FG valve opening is too small, it is not appropriate and will result in flooding of the flash tank, particularly for high refrigerant charges. So, the uncondensed ammonia (residual vapor) from condenser will go into the evaporator, causing a new steady-state condition with an evaporator exit quality of less than $x = 1$. Therefore, the proposed cycle with refrigerant heat exchanger (RHE) can overcome the above disadvantages.

Adding (RHE) is expected to decrease more the subcooled liquid refrigerant temperature of the two streams (state 7) by exchanging the heat with the cold vapor (state 9). However, this heat exchange could increase slightly the refrigerant vapor temperature entering the absorber (state 10) and ejector (state $10_B'$). The condensed refrigerant flow is separated into two streams. One stream flows to

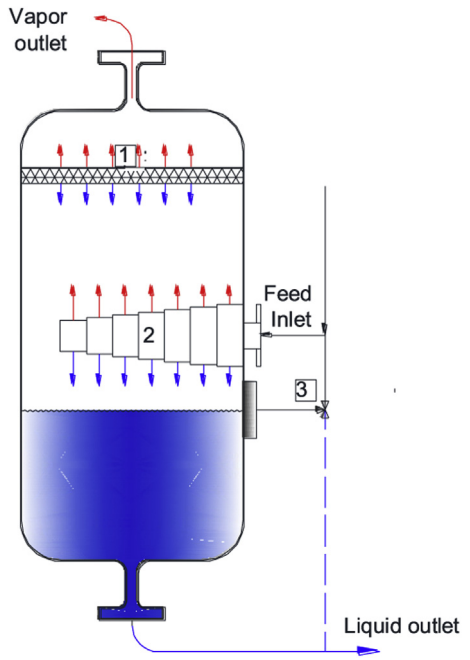

Fig. 3. Schematic diagram of flash tank. (1. De-entrainment meshes bed, 2. Distributor for liquid inlet, 3. Liquid level control valve).

the flash tank (state 6) and the second stream flows to the RHE (state 5). Both of these states are under same intermediate pressure. On the ejector side, the primary flow (ammonia vapor from the rectifier) and the secondary flow (i.e., ammonia vapor from the mixing of the evaporator and flash tank (state 17)) are mixed again and passed to the condenser (state 3).

4. Energy balance analysis of the proposed cycle

The operation of the proposed combined ejector–absorption cycle is characterized by the generator, condenser, absorber, and evaporator temperatures, as well as the refrigerant mass flow entering the ejector. The weak and strong solution concentrations at the absorber and generator are specified by their respective pressures and temperatures. Thus, the cycle can be analyzed as follows:

COP is used to measure the system performance:

$$\mathrm{COP} = \frac{Q_e}{Q_g + W_{me}} \tag{1}$$

Mass and energy conservation should be determined at each component to use Eq. (1).

- For the generator–absorber–rectifier loop

The mass and energy balances around the generator are as follows:

$$\dot{m}_{14} = \dot{m}_{13} + \dot{m}_{13A} + \dot{m}_{16} - \dot{m}_1 \quad \text{(total mass balance)} \tag{2}$$

$$\dot{m}_{14}\, X_{14} = \dot{m}_{13} X_{13} + \dot{m}_{13A} X_{13A} + m_{16} X_{16} - \dot{m}_1 Y_1 \quad (NH_3 \text{ mass balance}) \tag{3}$$

(where $X_{13} = X_{11}$ and $X_{13A} = X_{11}$).

$$Q_g = \dot{m}_1 h_1 + \dot{m}_{14}\, h_{14} - (\dot{m}_{13} h_{13} + \dot{m}_{16} h_{16} + \dot{m}_{13A} h_{13A}) \tag{4}$$

The fluid properties in this loop can be derived and developed as follows:

The liquid weak solution at state (14):

$$T_{14} = T_{gen},\ P_{14} = P_g,\ X_{14} = X_s(T_{gen}, P_g),\ \text{and}\ h_{14} = h_s(T_{gen}, X_{14}) \tag{5}$$

The vapor strong solution at point (1):

$$T_1 = T_{gen},\ P_1 = P_g,\ Y_1 = Y_s(P_g, X_{14}),\quad \text{and}\ h_1 = h_v(T_{gen}, Y_1) \tag{6}$$

The liquid that exits from the rectifier with vapor ammonia concentration is 0.996, so state (2) is derived as follows:

$$T_2 = T_{rect},\ P_2 = P_g,\quad \text{and}\ h_2 = h_r(T_2, P_2) \tag{7}$$

The remaining water in the solution returns to the generator, so state (16) is derived as follows:

$$T_{16} = T_{rect},\ P_{16} = P_g,\ X_{16} = (1 - Y_1),\quad \text{and}\ h_{16} = (T_{16}, X_{16}), \tag{8}$$

The saturated liquid strong solution at (11):

$$T_{11} = T_{abs},\ P_{11} = P_a,\ X_{11} = X_s(T_{abs}, P_a),\ \text{and}\ h_{11} = h_s(T_{11}, X_{11}), \tag{9}$$

Mass balance around the rectifier shell side

$$\dot{m}_1 = \dot{m}_2 + \dot{m}_{16} \tag{10}$$

$$\dot{m}_1\, Y_1 = \dot{m}_2 X_2 + \dot{m}_{16} X_{16} \quad (NH_3 \text{ mass balance}) \tag{11}$$

By solving and substituting Eqs. (10) and (11)

$$\dot{m}_{16} = (\dot{m}_1 Y_1 - \dot{m} X_2)/X_{16} \tag{12}$$

We need to calculate the work performed by the pump to determine the enthalpy at state (12):

$$T_{11} = T_{12},\ X_{11} = X_{12},\ P_{12} = P_g,\ v_{12} = v_s(T_{12}, X_{12}),\ \dot{m}_{11} = \dot{m}_{12} \tag{13}$$

$$h_{12} = h_{11} + [P_{12} - P_{11}] v_{12} \tag{14}$$

The absorbed liquid strong solution is pumped into two parts. One part is pumped into the rectifier, whereas the second part is pumped into the heat exchanger. Therefore, the mass flow rate on states (12A) and (12B) are as follows:

$$\dot{m}_{12} = \dot{m}_{12A} + \dot{m}_{12B},\ \dot{m}_{12} = 2\dot{m}_{12A}\quad \dot{m}_{12B} = \dot{m}_{13} \tag{15}$$

The energy balance around the rectifier can be expressed as follows to define state (13):

$$h_{13} = \frac{\dot{m}_1 h_1 + \dot{m}_{12B} h_{12B} - \dot{m}_2\, h_2 - \dot{m}_{16}\, h_{16}}{\dot{m}_{13}} \tag{16}$$

where $h_{12B} = h_{12}$

The effectiveness of the SHE (ε_{shx}) is assumed to calculate the temperature and determine the properties at state (14′):

$$T_{14'} = T_{12A}\varepsilon_{shx} + (1 - \varepsilon_{shx}) T_{14}\quad X_{14} = X_{14'},\ P_{14} = P_g,\ h_{14'} = h_s(T_{14'}, X_{14'}) \tag{17}$$

From the energy balance on the heat exchanger, state (13A) can then be defined as follows:

$$h_{13A} = \frac{\dot{m}_{14}h_{14} + \dot{m}_{12A}h_{12A} - \dot{m}_{14'}h_{14'}}{\dot{m}_{13A}} \quad (18)$$

Through the expansion valve, the fluid pressure decreases from high to low pressure. Thus:

$$P_{15} = P_a,\ X_{15} = X_{14'},\ \dot{m}_{14} = \dot{m}_{15},\ h_{14'} = h_{15} \quad (19)$$

- For Ejector-Flash tank-RHE loop

The ejector, flash tank, and RHE performance is described in this section. The flash tank pressure (P_{ft}) can be calculated from the following equation [20] to identify the flash tank pressure as defined in Ref. [25]:

$$P_{ft} = \sqrt{P_c\,P_e} \quad (20)$$

Concerning the cycle layout, the refrigeration vapor produced from the rectifier is used to generate the primary flow of the ejector and entrain the secondary vapor from the flash tank and evaporator. The vapor properties at state (2) are determined in Eq. (7). Given the above properties, the entrainment ratio (i.e. $\omega = \dot{m}_{17}/\dot{m}_2$) of the ejector can be determined from the following relationship:

$$\omega = f\left(P_2,\ T_2,\ P_{17},\ T_{17},\ P_3,\ \frac{A_t}{A_k}\right) \quad (21)$$

Detailed formulations of the above function are described in Refs. [10,25]. The performance evolution procedure for the ejector is used to calculate the entrainment ratio. Iteration mathematical calculation is performed to determine the entrainment ratio that defines the ejector capacity and performance. Once ω is known, the properties at states (3) are derived from the mixing process as follows:

$$\dot{m}_{17} = \omega\dot{m}_2 \quad (22)$$

$$\dot{m}_3 = (1+\omega)\dot{m}_2 \quad (23)$$

$$h_3 = \frac{h_2 + \omega h_{17}}{1+\omega} \quad (24)$$

The fluid at (4) coming from the condenser can be specified as follows:

$$T_4 = T_{cond},\ \dot{m}_4 = \dot{m}_3,\ P_4 = P_r\,(T_4),\ h_4 = h_r(T_4, P_4) \quad (25)$$

This fluid then undergoes pressure reduction through an expansion valve and split into two parts to enter the flash tank and RHE:

$$P_6 = P_{ft},\ T_6 = T_r\,(P_6),\ h_6 = h_4,\ \dot{m}_6 = \dot{m}_4 - \dot{m}_5 \quad (26)$$

Inside the flash tank, the subcooled liquid and saturated vapor separates as follows:

$$P_{6A} = P_{ft},\ T_{6A} = T_r\,(P_6),\ h_{6A} = h_{(6A)l} = h_l\left(T_{ft}\right),\quad h_{6B} = h_{(6B)v} = h_r\left(T_{ft}\right) \quad (27)$$

$$\dot{m}_{6A} = \frac{\dot{m}_{6B}(h_6 - h_{6B})}{(h_{6A} - h_6)} \quad (28)$$

The properties of the saturated vapor ammonia (17) entrained by the ejector are determined from the following:

$$h_{17} = \frac{\dot{m}_{6B'}h_{6B'} + \dot{m}_{10B'}h_{10B'}}{\dot{m}_{17}},\ T_{17} = h_v\,(T_{17}),\ P_{17} = P_e \quad (29)$$

The properties at point (7) can also be specified as follows:

$$\dot{m}_7 = \dot{m}_{6A} + \dot{m}_5,\ \dot{m}_4 = 2\dot{m}_5,\ h_4 = h_5,\ P_7 = P_{6A} \quad (30)$$

$$h_7 = \frac{\dot{m}_5 h_5 + \dot{m}_{6A}\,h_{6A}}{\dot{m}_7},\ T_7 = h_r\,(T_7) \quad (31)$$

The RHE performance is expressed in terms of effectiveness ε_{rhx}. The subcooled liquid at state (7′) is derived using the above values as follows:

$$T_{7'} = T_9\varepsilon_{rhx} + (1-\varepsilon_{rhx})T_7,\ \dot{m}_{7'} = \dot{m}_7,\ X_7 = X_{7'},\ h_{7'} = h_r(T_{7'}, P_{7'}) \quad (32)$$

The properties of the subcooled liquid after the expansion valve at point (8):

$$h_8 = h_{7'},\ P_8 = P_e,\ \dot{m}_{7'} = \dot{m}_8,\ T_8 = h_r(T_8) \quad (33)$$

The properties of the vapor at (9) coming from the evaporator can be determined as follows:

$$T_9 = T_{evp},\ P_9 = P_e,\ \dot{m}_8 = \dot{m}_9,\ h_9 = h_r(T_9, P_9) \quad (34)$$

By applying the heat balance on the RHE, point (10) can be defined as follows:

$$h_{10} = \frac{\dot{m}_7 h_7 + \dot{m}_9 h_9 - \dot{m}_{7'}h_{7'}}{\dot{m}_{10}} \quad (35)$$

$$T_{10} = h_r\,(T_{10}),\ P_{10} = P_e,\ \dot{m}_{10} = \dot{m}_9$$

The mass flow rate for points (10B) and (6B) can be determined as follows:

$$\dot{m}_{10B} = \dot{m}_{10} - \dot{m}_{10A},\ \dot{m}_{17} = \dot{m}_{10B'} + \dot{m}_{6B'},\ \dot{m}_{6B'} = \dot{m}_{6B},\quad \dot{m}_{10B} = \dot{m}_{10B'},\quad \dot{m}_{10A} = \dot{m}_2 \quad (36)$$

The vapor at (10A) entering the absorber can also be specified as follows:

$$P_{10A} = P_e,\ T_{10} = T_{10A},\ h_{10} = h_{10A} \quad (37)$$

Finally, the energy balance for the absorber, condenser, and evaporator yield are as follows:

$$Q_e = \dot{m}_9(h_9 - h_8) \tag{38}$$

$$Q_c = (1 + \omega)\dot{m}_2(h_3 - h_4) \tag{39}$$

$$Q_a = \dot{m}_{10A}h_{10A} + \dot{m}_{15}h_{15} - \dot{m}_{11}h_{11} \tag{40}$$

The RHE effect on refrigeration capacity can be quantified in terms of a relative capacity change index (RCI) as defined in [29]:

$$RCI = \left(\frac{Capacity - Capacity_{nohx}}{Capacity_{nohx}}\right) \times 100\% \tag{41}$$

where Capacity is the refrigeration capacity with RHE, $Capacity_{nohx}$ is the refrigeration capacity for a system operating at the same condensing and evaporating temperature without an RHE.

5. Results and discussion

It is worthy to note that this article is an extension work of our previous research [25]. In this work, the mathematical procedure is similar to that adopted in Ref. [25]. So, there is no need to include the validation of the present Mathematical Procedures as it is already confirmed in Ref. [25].

A computer simulation program for the NH_3/H_2O mixture has been developed based on Section 4 above. The operation condition range of the proposed cycles are T_{gen} = 60–120 °C, $T_{cond} = T_{abs}$ = 20–50 °C, T_{evp} = −15 to 15 °C, whereas the mass flow rate of the refrigerant is 0.0166 kg/s. The solution and refrigerant heat exchangers effectiveness are 0.5 and 0.6, respectively. Given the operation condition and cooling load, the software predicts the system performance, ejector performance, and optimum design map for the system. The temperature, pressure and mass flow rate evaluations of the proposed cycle is listed in Table 2-Appendix–A.

The potential and significance of the proposed cycle compared with previous cycle is discussed in details below. The PTx Dühring diagram for the proposed cycle and the ordinary combined cycle is shown in Fig. 4. The locations of liquid and the vapor states based on (*T*,*x*) and (*P*,*x*) are illustrated also in this same figure. The numbering marked in blue (in the web version) refer to the ordinary combined cycle points while the numbering marked in black refers to the proposed combined cycle.

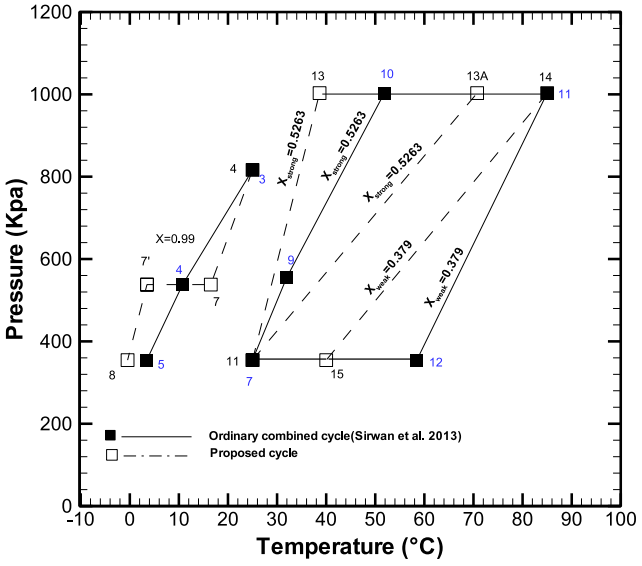

Fig. 4. PTx diagram for the proposed and ordinary combined cooling cycles.

The dashed and continuous lines represent the proposed and ordinary combined cycles respectively. The weak and strong solution concentrations are 0.379 and 0.5263 respectively. In the proposed cycle, the strong solution is heated by SHE from 11 to 13A, while the weak solution is cooled at 14 and 15. While in the ordinary combined cycle, the continuous line 7–9–10 is heating process and 11–12 is cooling process. This shifting in the PTx diagram is due to the new re-arrangement of streamlines of the strong solution.

At the rectifier, the liquid strong solution is partially heated in 11–13 and the vapor is cooled by the strong solution pumped from the absorber. Moreover, it can be seen that there is a temperature shift in the liquid refrigerant streamlines (from ordinary cycle 3–4–5 to the proposed cycle 4–7–7′–8). This shift is due to the sub-cooling effect of the RHE at the evaporator inlet and outlet.

5.1. Effect of different operating temperatures on the COP

Variation of COP values versus the generator/evaporator/condenser/absorber operating temperature range for the basic cycle, combined cycle (Ejector + Ft), and the proposed cycle are shown in Fig. 5(a)–(d). The COP of the proposed cycle is the highest, and its trend is similar to the basic cycle. This trend is similar to the trend of previous studies [10,41,42].

Although the COP results of the proposed cycle are higher than the combined cycle, this is insufficient to determine whether that the higher performance values of the proposed cycle are a significant enhancement or not. Therefore, the COP results of the proposed cycle must show a significant difference compared with the ordinary combined cycle. Statistical paired *t*-test tool is adopted to verify if the enhancement of the performance that occurred with the proposed cycle is larger than would be expected by chance. If so, then a statistically significant change has occurred. From the results of the paired *t*-test, an extremely statistically significant "performance difference" is observed between the proposed and the ordinary combined cycles. The results of *t*-test is shown in Table 3-Appendix–A.

5.2. Effect of the operating temperatures on thermal loads

The effect of the different operating temperature ranges of the generator and evaporator thermal loads for both the combined and proposed cycles are shown in Figs. 6 to 9. As shown in Fig. 6, the thermal load of the combined cycle starts decreasing gradually until T_g = 90 °C, and then the thermal load increases again. Based on this design, the generator thermal load is no longer useful after T_g = 90 °C. In the proposed cycle, when the generator temperature increases, the generator thermal load (Q_{gen}) starts to decrease gradually until T_g = 100 °C. The thermal load then remains almost constant.

If the generator temperature increases, the ammonia vapor concentration leaving the generator and the weak solution temperature increase. Thus, the enthalpy (h_{13A}) is increased by the strong solution in the SHE. The generator thermal load is decreased both by decreasing the circulation ratio and increasing the enthalpy in the strong solution [34]. The proposed cycle evidently has a lower generator thermal load compared with the combined cycle studied by Sirwan et al. [25]. The generator temperature also does not affect the ejector entrainment ratio and evaporator thermal load. Finally, the new design can add advantages to the proposed

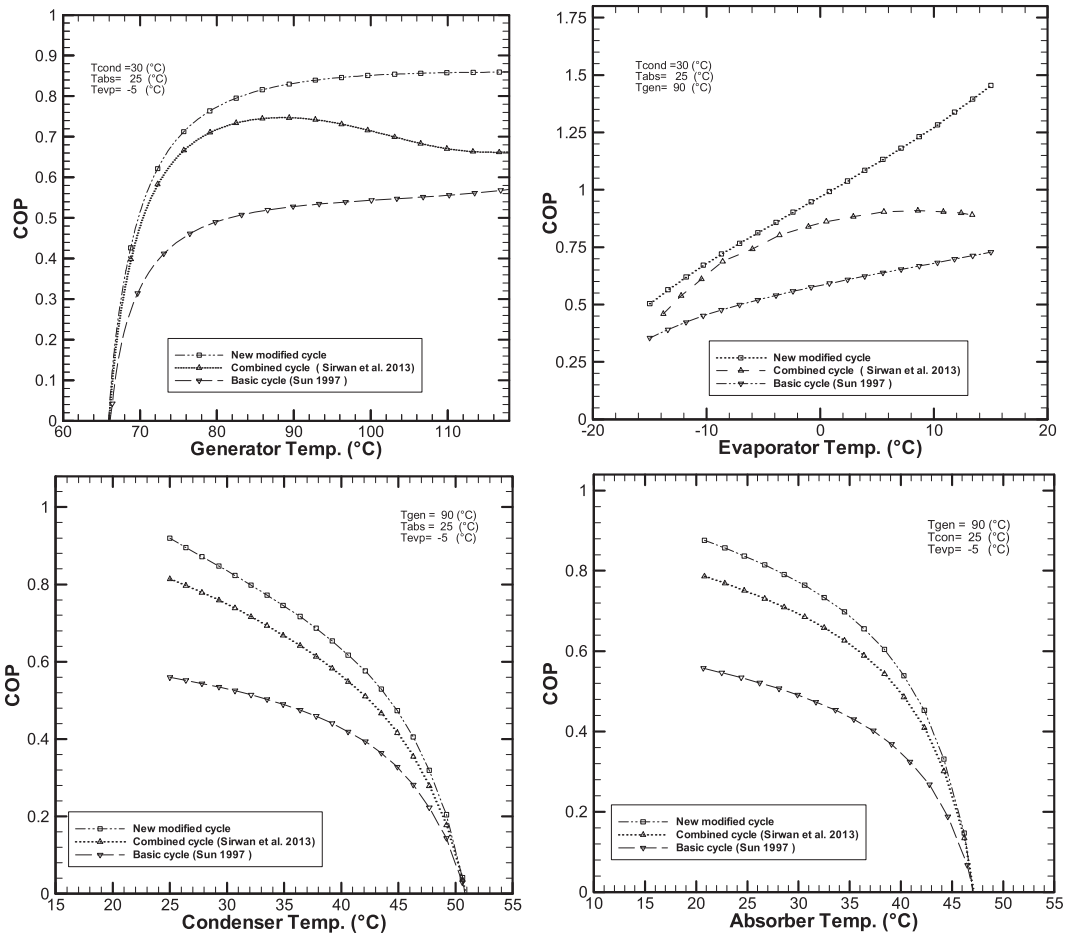

Fig. 5. COP variation versus the operating temperature ranges of the main components of the absorption cooling cycle.

cycle under the generator temperature range compared with the combined cycle.

The variations in evaporator temperature with the thermal loads are shown in Fig. 7. The generator thermal load decreases with an increase in evaporator temperature, whereas the evaporator load increases when the evaporator temperature increases. The entrainment ratio ω also increases rapidly as the evaporator temperature increases because an increase in the evaporator

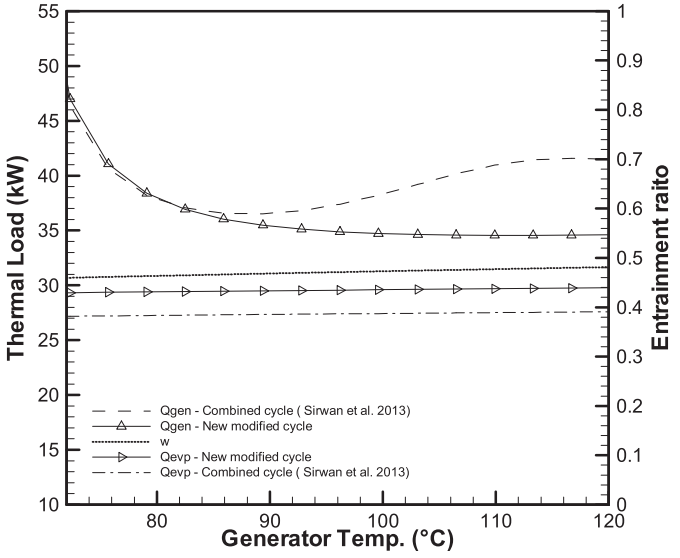

Fig. 6. Variation of thermal loads and entrainment ratio versus generator temperature.

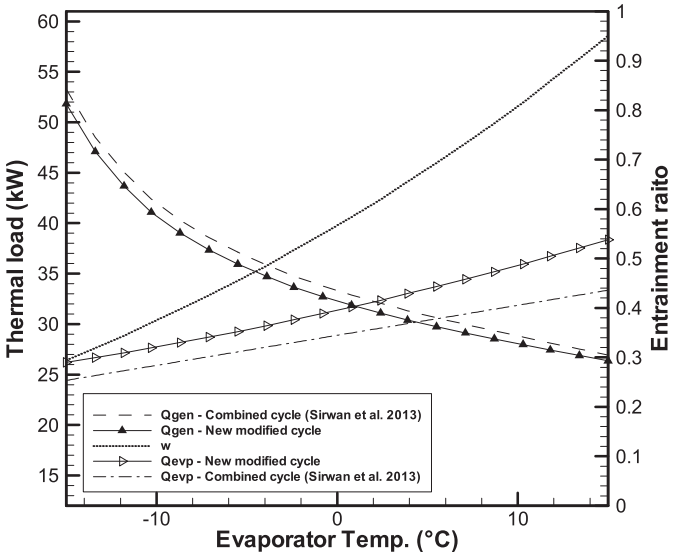

Fig. 7. Thermal load and entrainment ratio versus evaporator temperature.

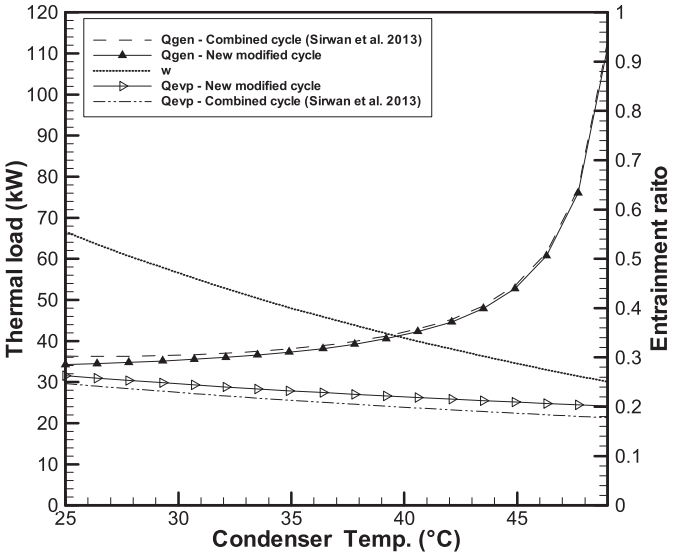

Fig. 8. Thermal load and entrainment ratio versus condenser temperature.

pressure and flash tank causes an increase in the vapor flow rate entering the ejector as the primary flow rate remains unchanged. These results are similar to previous works [10,42]. However, cooling cycles operating at high evaporator temperatures have no practical meaning in refrigeration or air-conditioning [12,42]. In the proposed cycle, the FG valve replaced the booster at the flash tank vapor streamline to adjust the pressure in the ejector secondary flow rate. By employing RHE, the refrigerant entering the evaporator is subcooled because the refrigerant enters the evaporator at a relatively low enthalpy, whereas the saturated vapor leaving the evaporator and entering the absorber and ejector is heated. Thus, the thermal loads of these components increase slightly. The results show that the proposed cycle has a lower generator thermal load and a higher cooling capacity than that of the combined cycle studied by Sirwan et al. [25].

The variations in the thermal loads under the condenser temperature range are shown in Fig. 8. When the condenser temperature increases, the high pressure of the condenser increases and the strong solution concentration decreases [34]. With the increasing condenser pressure, the amount of saturated liquid enthalpies leaving the condenser also increases. This condition leads to a decrease in the condenser thermal load. By decreasing the strong solution concentration, the circulation ratio of the flow rate also increases. In this case, the generator thermal load increases. These results agree with previous studies [25,34]. The entrainment ratio for the ejector also decreases, so the pressure or the ejector back-pressure increases with constant evaporator pressure (i.e., secondary flow pressure), which leads to a decrease in the ejector efficiency. When the condenser pressure is increased higher than the critical value, the transverse shock tends to move backward into the mixing chamber and interferes with the mixing of the primary and secondary fluids. The secondary flow is no longer choked, so the secondary flow varies and the entrainment ratio begins drop. If the condenser pressure is further increased, the flow reverses back into the evaporator and the ejector loses its function completely [12].

The variation in the absorber temperature on the thermal loads and entrainment ratio are shown in Fig. 9. By increasing the absorber temperature, the strong solution concentration approaches the weak solution concentration and the circulation ratio increases. Therefore, the generator thermal load increases. However, the evaporator thermal load is unaffected under the absorber temperature range and remains constant for both cycles.

Based on the results of this section, the proposed cycle generally shows lower generator and absorber thermal loads and higher evaporator thermal load (i.e., cooling effect) than that in the combined cycle before modifications.

5.3. Heat exchanger effect

RCI versus heat exchanger effectiveness at a fixed generator temperature of 90°°C is presented in Fig. 10, for different operating conditions. RCI quantifies the RHE effect on refrigeration capacity, whereas RHE effectiveness represents its performance. As the RHE effectiveness increases, the refrigerant entering the evaporator is subcooled because the liquid refrigerant reaching the expansion valve at a lower temperature rejects its energy to the vapor refrigerant leaving the evaporator. The relative capacity increases significantly and linearly as the heat exchanger effectiveness increases. The figure also shows that as the RHE effectiveness increases, the effect of operating conditions of condenser/absorber/

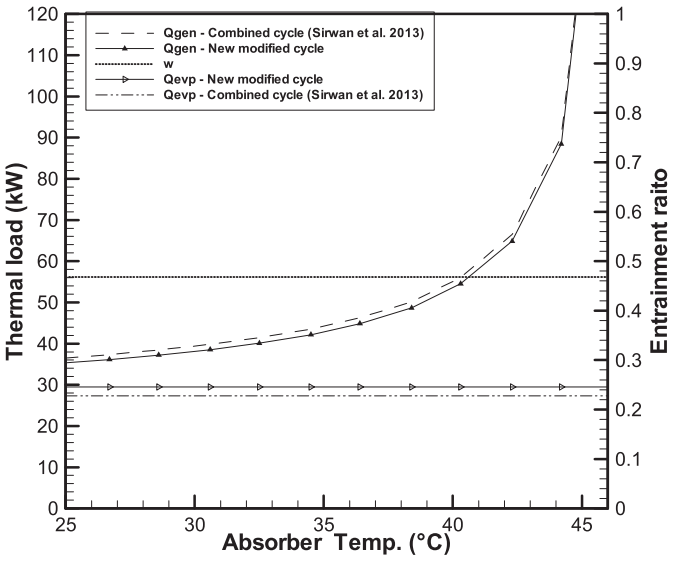

Fig. 9. Variation of thermal loads and entrainment ratio versus absorber temperature.

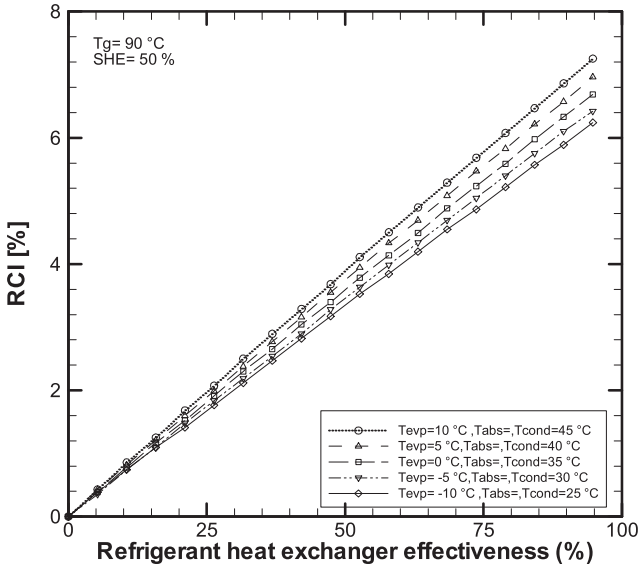

Fig. 10. System capacity changes as a function of RHE effectiveness.

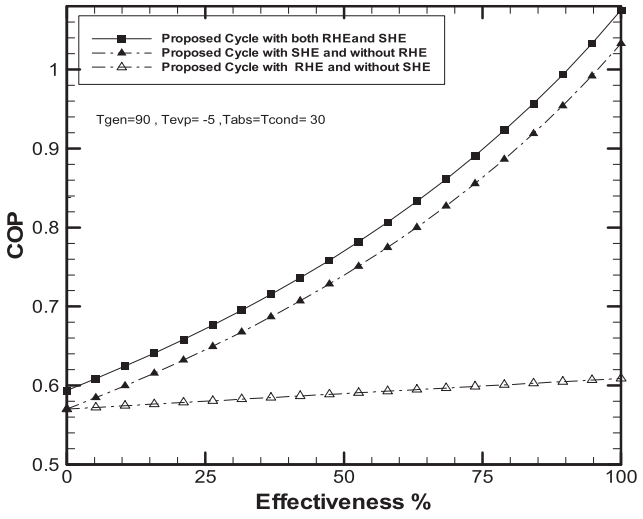

Fig. 11. COP versus heat exchanger effectiveness at $T_{gen} = 90\ ^{\circ}C$, $T_{cond} = T_{abs} = 30\ ^{\circ}C$, $T_{evp} = -5\ ^{\circ}C$.

evaporator on RCI increases; where the maximum increase is found at higher operating temperatures. However, the effect of operating conditions of condenser/absorber/evaporator on RCI is considered minor compare to the influence of RHE effectiveness. In this study, the RHE effectiveness is 60%. Thus, the maximum RCI value that can be achieved is 4.85% as shown in Fig. 10.

Fig. 11 shows the COP of the cycle versus the effectiveness of heat exchangers (RHE, SHE) at different scenarios. The first scenario assumed that the proposed cycle is (with RHE and without SHE). In this case, the COP of the proposed cycle is increasing slightly as the effectiveness of RHE increases. The second scenario assumed that the proposed cycle is (with SHE and without RHE). In this case, the COP of the proposed cycle is increasing significantly as the effectiveness of SHE increases and compare to the COP at scenario 1. The third scenario assumed that the proposed cycle is (with SHE and RHE). In this case, the COP of the proposed cycle is also increasing significantly as the effectiveness of both heat exchangers increases. As shown in Fig. 11, at any heat exchanger effectiveness value, it can be seen that the best COP values is obtained under scenario 3, the second best COP values is obtained under scenario 2, and the worst COP values is obtained under scenario 1. In the literature, the RHE effect improves the COP by approximately 8% as reported in Ref. [32].

6. Conclusion

In this study, the energy balance analysis of a modified combined ejector-flash tank-absorption refrigeration system using NH_3/H_2O as the working fluid was performed. The theoretical performances of the modified and ordinary combined cycle were compared. The overall COP improvement of the proposed combined cycle increased approximately 12.2% compare to ordinary combined cycle. The stream re-arrangement at solution heat exchanger and rectifier assist the generator partially, thus reducing the thermal load of generator and absorber requirement, and consequently, improves the COP. The obtained COP improvement when utilizing the energy heat recovery in the absorber and rectifier is found 8%. The COP improvement by adding the RHE is found 4.2%, and the maximum increase in RCI is found 4.85%. Finally, the proposed cycle was able to minimize the energy consumption at the generator and absorber and improving the quality of the refrigerant that enters the evaporator, especially when the condenser temperature is high compare to evaporator temperature. For future work, dealing with secondary flow pressure is still subject for further investigation. So, the coming article will discuss the effect of operating two ejectors that can work under two levels of secondary pressure i.e. flash tank pressure and evaporator pressure on the COP of the proposed cycle.

Appendix–A

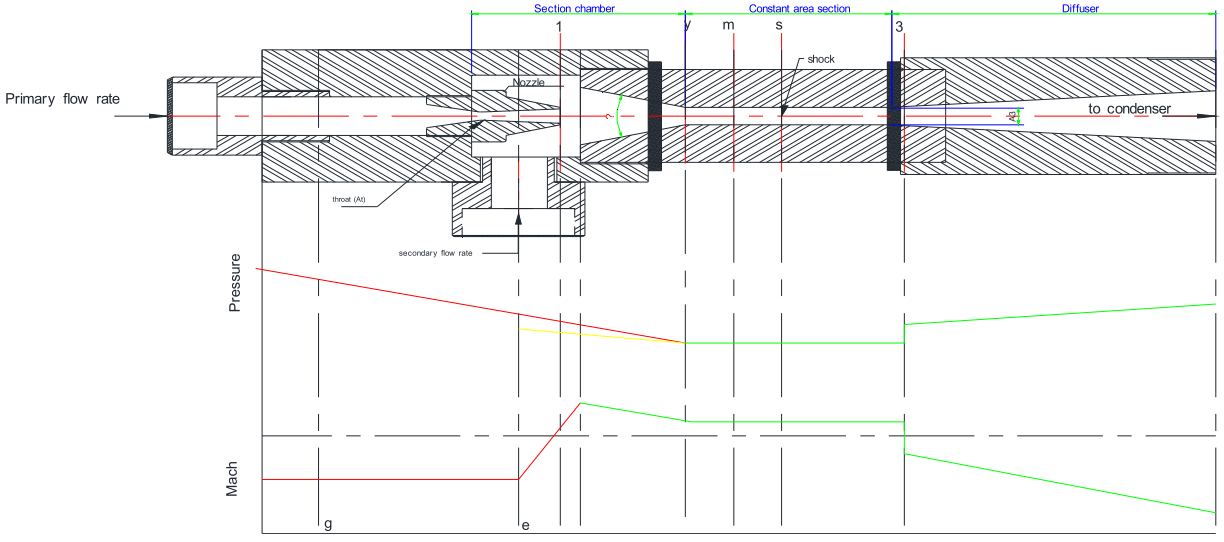

Fig A-1. Ejector design schematic.

Table A-1
State points for ejector.

	P	e	1	$y-y$	$m-m$	$s-s$	c	ω
Pressure	1003	3.544	5.839	1.922	1.922	6.378	8.165	0.6869
Temperature	85	−5						
Velocity				22.74	22.74	21.77	12.71	
Mach number	1	1	1.835	1.755	1.743	1.743	0.6212	

Table A-2
State points for the proposed combined cooling cycle. (T_{gen} = 85 (°C), $T_{cond} = T_{abs}$ = 25 (°C), T_{evp} = −5 (°C)).

State points	T_i (°C)	P_i (kPa)	X_i (%)	$\dot{m}_i$ (kg/s)	h_i (kJ/kg)
1	85	1003	0.9388	0.01775	1528
2	55.05	1003	0.996	0.01667	1486
3	–	816.5	0.996	0.02811	1496
4	25	816.5	0.996	0.02811	315.9
5	–	537.9	0.996	0.01406	315.9
6	–	537.9	0.996	0.01406	315.9
6A	–	537.9	0.996	0.01304	225.7
6B	–	537.9	0.996	0.001018	1471
7	16.04	537.9	0.996	0.0271	272.5
7′	3.45	537.9	0.996	0.0271	214.1
8	–	354.4	0.996	0.0271	214.1
9	−5	354.4	0.996	0.0271	1457
10	7.85	354.4	0.996	0.0271	1515
10A	7.85	354.4	0.996	0.01667	1515
10B	7.85	354.4	0.996	0.01043	1515
11	25	354.4	0.5263	0.06983	−140.7
12	–	1003	0.5263	0.06983	−139.9
12B	–	1003	0.5263	0.03492	−139.9
12A	–	1003	0.5263	0.03492	−139.9
13	38.65	1003	0.5263	0.03492	−78.38
13A	70.75	1003	0.5263	0.03492	74.4
14	85	1003	0.379	0.05316	141
14′	55	1003	0.379	0.05316	0.2235
15	–	354.4	0.379	0.05316	0.2235
16	55	1003	0.06116	0.001085	183.4
17	8.5	354.4	0.996	0.001145	1515

Paired t-test results

Table A-3
Test results for the COP of the proposed cycle and ordinary combined cycle.

Group	After modification	Before modification
Mean COP	0.7245253	0.6131793
SD	0.1654419	0.1267542
SEM	0.0302054	0.0231421
N	30	30

- *P* value and statistical significance:
  The two-tailed *P* value is less than 0.0001
  By conventional criteria, this difference is considered to be extremely significant
- Confidence interval
  The mean of new modified cycle minus ordinary combined cycle equals 0.1113460
  95% confidence internal of this difference: from 0.0881871 to 0.1345049
- Intermediate values used in calculations
  t = 9.8333, df = 29, Standard error of difference = 0.011

References

[1] P. Srikhirin, S. Aphornratana, S. Chungpaibulpatana, A review of absorption refrigeration technologies, Renew. Sustain. Energy Rev. 5 (2001) 343–372.
[2] K.E. Herold, R. Radermacher, S.A. Klein, Absorption Chillers and Heat Pumps, CRC Press, NewYork, 1996.
[3] R.D. Misra, P.K. Sahoo, A. Gupta, Thermoeconomic evaluation and optimization of an aqua-ammonia vapour-absorption refrigeration system, Int. J. Refrig. 29 (2006) 47–59.
[4] J. Fernández-Seara, M. Vázquez, Study and control of the optimal generation temperature in NH_3–H_2O absorption refrigeration systems, Appl. Therm. Eng. 21 (2001) 343–357.
[5] J.M. Gordon, K. Choon Ng, High-efficiency solar cooling, Sol. Energy 68 (2000) 23–31.
[6] L.A. Howe, R. Radermacher, K.E. Herold, Combined cycles for engine-driven heat pumps, Int. J. Refrig. 12 (1989) 21–28.
[7] L. Åhlby, D. Hodgett, T. Berntsson, Optimization study of the compression/absorption cycle, Int. J. Refrig. 14 (1991) 16–23.
[8] S. Göktun, Optimal performance of a combined absorption and ejector refrigerator, Energy Convers. Manag. 40 (1999) 51–58.
[9] S. Aphornratana, I.W. Eames, Experimental investigation of a combined ejector-absorption refrigerator, Int. J. Energy Res. 22 (1998) 195–207.
[10] D.-W. Sun, I.W. Eames, S. Aphornratana, Evaluation of a novel combined ejector-absorption refrigeration cycle — I: computer simulation, Int. J. Refrig. 19 (1996) 172–180.
[11] D.S. Ward, Solar absorption cooling feasibility, Sol. Energy 22 (1979) 259–268.
[12] K. Chunnanond, S. Aphornratana, Ejectors: applications in refrigeration technology, Renew. Sustain. Energy Rev. 8 (2004) 129–155.
[13] J.M. Abdulateef, K. Sopian, M.A. Alghoul, M.Y. Sulaiman, Review on solar-driven ejector refrigeration technologies, Renew. Sustain. Energy Rev. 13 (2009) 1338–1349.
[14] X. Chen, S. Omer, M. Worall, S. Riffat, Recent developments in ejector refrigeration technologies, Renew. Sustain. Energy Rev. 19 (2013) 629–651.
[15] J. Wang, G. Chen, H. Jiang, Study on a solar-driven ejection absorption refrigeration cycle, Int. J. Energy Res. 22 (1998) 733–739.
[16] K. Cizungu, M. Groll, Z.G. Ling, Modelling and optimization of two-phase ejectors for cooling systems, Appl. Therm. Eng. 25 (2005) 1979–1994.
[17] C. Vereda, R. Ventas, A. Lecuona, M. Venegas, Study of an ejector-absorption refrigeration cycle with an adaptable ejector nozzle for different working conditions, Appl. Energy 97 (2012) 305–312.
[18] J. Heo, M.W. Jeong, Y. Kim, Effects of flash tank vapor injection on the heating performance of an inverter-driven heat pump for cold regions, Int. J. Refrig. 33 (2010) 848–855.
[19] X. Shuxue, M. Guoyuan, Experimental study on two-stage compression refrigeration/heat pump system with dual-cylinder rolling piston compressor, Appl. Therm. Eng. 61 (2013) 803–808.
[20] H. Cho, C. Baek, C. Park, Y. Kim, Performance evaluation of a two-stage CO_2 cycle with gas injection in the cooling mode operation, Int. J. Refrig. 32 (2009) 40–46.
[21] J. Heo, M.W. Jeong, C. Baek, Y. Kim, Comparison of the heating performance of air-source heat pumps using various types of refrigerant injection, Int. J. Refrig. 34 (2011) 444–453.
[22] G.Y. Ma, H.X. Zhao, Experimental study of a heat pump system with flash-tank coupled with scroll compressor, Energy Build. 40 (2008) 697–701.
[23] B. Wang, W. Shi, L. Han, X. Li, Optimization of refrigeration system with gas-injected scroll compressor, Int. J. Refrig. 32 (2009) 1544–1554.
[24] S. Elbel, P. Hrnjak, Flash gas bypass for improving the performance of transcritical R744 systems that use microchannel evaporators, Int. J. Refrig. 27 (2004) 724–735.
[25] R. Sirwan, M.A. Alghoul, K. Sopian, Y. Ali, J. Abdulateef, Evaluation of adding flash tank to solar combined ejector–absorption refrigeration system, Sol. Energy 91 (2013) 283–296.
[26] R. Sirwan, M.A. Alghoul, K. Sopian, Y. Ali, Thermodynamic analysis of an ejector-flash tank-absorption cooling system, Appl. Therm. Eng. 58 (2013) 85–97.
[27] S.A. Klein, D.T. Reindl, K. Brownell, Refrigeration system performance using liquid-suction heat exchangers, Int. J. Refrig. 23 (2000) 588–596.
[28] R. Mastrullo, A.W. Mauro, S. Tino, G.P. Vanoli, A chart for predicting the possible advantage of adopting a suction/liquid heat exchanger in refrigerating system, Appl. Therm. Eng. 27 (2007) 2443–2448.
[29] P.A. Domanski, D.A. Didion, J.P. Doyle, Evaluation of suction-line/liquid-line heat exchange in the refrigeration cycle, Int. J. Refrig. 17 (1994) 487–493.
[30] ASHRAE, Fundamental. ASHRAE Handbook, ASHRAE, Atlanta, 2009.
[31] W.T. Hanna, et al., Pinch-point analysis: an aid to understanding the GAX absorption cycle, ASHRAE Tech. Data Bull. 11 (1995).
[32] G. Holldorff, Revisions up absorption refrigeration efficiency, Hydrocarbon Process. 58 (1979) 149.
[33] ASHRAE, Fundamental. ASHRAE Handbook, ASHRAE, Atlanta, 1997.
[34] O. Kaynakli, M. Kilic, Theoretical study on the effect of operating conditions on performance of absorption refrigeration system, Energy Convers. Manag. 48 (2007) 599–607.
[35] S. Kandlikar, A new absorber heat recovery cycle to improve COP of aqua-ammonia absorption refrigeration system, ASHRAE Trans. 88 (1982) 141–158.
[36] S.C. Kaushik, R. Kumar, A comparative study of an absorber heat recovery cycle for solar refrigeration using NH_3-refrigerant with liquid/solid absorbents, Int. J. Energy Res. 11 (1987) 123–132.
[37] P. Bourseau, R. Bugarel, Absorption–diffusion machines: comparison of the performances of NH_3H_2O and NH_3NaSCN, Int. J. Refrig. 9 (1986) 206–214.
[38] D.Y. Goswami, Solar thermal power technology: present status and ideas for the future, Energy Sources 20 (1998) 137–145.
[39] F. Xu, D. Yogi Goswami, S.S. Bhagwat, A combined power/cooling cycle, Energy 25 (2000) 233–246.
[40] J. Pátek, J. Klomfar, Simple functions for fast calculations of selected thermodynamic properties of the ammonia–water system, Int. J. Refrig. 18 (1995) 228–234.
[41] M.I. Karamangil, S. Coskun, O. Kaynakli, N. Yamankaradeniz, A simulation study of performance evaluation of single-stage absorption refrigeration system using conventional working fluids and alternatives, Renew. Sustain. Energy Rev. 14 (2010) 1969–1978.
[42] D.-W. Sun, Solar powered combined ejector-vapour compression cycle for air conditioning and refrigeration, Energy Convers. Manag. 38 (1997) 479–491.